Low-frequency thermohaline variability in the Subtropical South Atlantic pycnocline during 2002-2013

Nicolas Kolodziejczyk[1], Gilles Reverdin[1], Fabienne Gaillard[2] and Alban Lazar[1]

submitted to *Geophysical Research Letters*

[1]Sorbonne Universités (UPMC, Univ Paris 06)-CNRS-IRD-MNHN, LOCEAN Laboratory, 4 place Jussieu, F-75005, Paris, France

[2]Ifremer, Laboratoire de Physique des Océans, UMR 6523-CNRS-Ifremer-IRD-UBO, Plouzané, France.

Corresponding author: Dr. Nicolas Kolodziejczyk, E-mail: nicolas.kolodziejczyk@gmail.com

ABSTRACT

Low-frequency variability of spiciness is observed in the Subtropical South Atlantic over the period 2002-2013 with the Argo gridded product ISAS. Within the pycnocline, spiciness anomalies propagate at a mean speed of 0.04±0.02 $m.s^{-1}$, the same speed as the gyre mean circulation, from the Agulhas Retroflection region off South Africa (~35°S-20°E) towards the South American coast (~18°S-35°W). After 2010, propagation is still found, but stationary local spiciness generation is also found over the Subtropical South Atlantic. This spiciness increase is associated with high values of vertical Turner angle below the mixed layer base during late winter. This suggests spice injection resulting from penetrative convective mixing due to air-sea buoyancy loss. These features may have an impact on the low-frequency warm and salty signal produced by the Agulhas leakage in Subtropical South Atlantic and the upper branch of the Atlantic Meridional Overturning Circulation.

1 Introduction

The transport of warm and salty Indian Ocean waters into the Atlantic Ocean – the Agulhas leakage – plays a crucial role in the global oceanic circulation and the evolution of past and future climates [*Biastoch et al.*, 2008; *Beal et al.*, 2011]. These water masses are constituted from intermediate [*Rusciano et al.*, 2012] and thermocline [*Gordon*, 1986] water masses that provide the main sources of heat and salt of the warm upper limb of the South Atlantic Meridional Overturning Circulation (AMOC; [*Gordon*, 1986; *Gordon,* 1996; *Speich et al.*, 2001; *Friocourt et al.*, 2005; *Speich et al.*, 2007]). The Subtropical South Atlantic (SSA) pycnocline water masses are embedded in the larger wind driven South Hemisphere 'Supergyre ' that connects the Indo-Atlantic basin via the Agulhas Current and Leakage in the south-eastern South Atlantic [*de Ruijter*, 1982; *Lutjeharms and van Ballegooyen*, 1988] and may exchange water masses with the Southern Ocean [*Lutjeharms*, 1988; *Dencausse et al.*, 2010ab]. Although the Agulhas salt anomalies are largely density compensated as they enter the Subtropical South Atlantic, progressive atmospheric heat loss creates an increasing positive density anomaly as salt is left behind and waters are advected northward [*Weijer et al.*; 2002; *Haarsma et al.*, 2011]. The density-compensated potential temperature and salinity variations of sea water along isopycnal surfaces are addressed as spiciness variations [*Veronis*, 1976; *Lazar et al*., 2001]. Thus, in the South Atlantic pycnocline, a fraction of the Agulhas warm and salty interannual-to-decadal signal may be transported northward with the mean subtropical gyre circulation as density compensated anomalies. Moreover, the AMOC return surface waters are embedded in the shallow wind-driven Subtropical-Tropical Cells (STCs) [*Zhang et al.*, 2002], thus likely to affect the tropical circulation and climate [*Hazelager et al.*, 2003; *Hazeleger and Drijfhout*, 2006; *Haarsma et al.*, 2011].

In contrast, recent studies have shown that a part of SSA pycnocline spiciness signal may be generated by spice

injection events at the base of the mixed layer, which occur under the late winter upright convection enhanced by a destabilizing vertical salinity gradient (generally found poleward of the subtropical salt maxima) [*Yeager and Large*, 2007]. This process generates Strongly Density Compensated (SDC) layers below the late winter mixed layer [*Liu et al.*, 2009], which affect the permanent pycnocline spiciness signal [*Kolodziejczyk and Gaillard*, 2012, 2013]. The SDC are characterized by the highest value of the vertical Turner angle [*Ruddick*, 1983] computed as:

$$Tu = \operatorname{atan}\left(\frac{\alpha \partial_z T + \beta \partial_z S}{\alpha \partial_z T - \beta \partial_z S}\right) \quad (1)$$

where T and S are the temperature and salinity, respectively; α and β are the coefficients of expansion for temperature and salinity, respectively. When a destabilizing salinity gradient is concomitant with a stabilizing temperature gradient, Tu > 45°. If Tu > 71.6° the process of double-diffusion starts to be active [*St Laurent and Schmitt*, 1999], when Tu tends to 90° the buoyancy effects of $\partial_z T > 0$ and $\partial_z S > 0$ are of opposite signs leading to a perfect density compensation. In the subtropical regions, the spice injection process is mainly driven by the seasonal and interannual variability of the winter air-sea buoyancy loss [*Kolodziejczyk and Gaillard*, 2013].

The high-quality data profiles from Argo floats collected in the past decade provides an invaluable tool to monitor subsurface spiciness variations [*Sasaki et al.*, 2010; *Kolodziejczyk and Gaillard*, 2012]. The Subtropical South Atlantic is now sufficiently sampled to monitor the low frequency - the interannual-to-decadal - thermohaline variability in the permanent pycnocline and to address its potential modulation by the Agulhas leakage and interannual atmospheric conditions.

The paper is organized as follows: in Section 2, evidences of propagation of density-compensated signal emanating from Agulhas Retroflection region are shown within the SSA pycnocline. In section 3, the possible impact of the local atmospheric forcing on density-compensated signal in the pycnocline in the SSA is discussed. In the final section, the results are summarized and discussed, as well as remaining questions.

2 Observation of spiciness variability

In this study, the low-frequency spiciness variations over the SSA (50°W– 20°E, 40°S–5°S) is investigated using the ISAS (In Situ Analysis System) 2002-2013 temperature and salinity gridded fields mainly based on Argo data [*Gaillard et al.*, 2009]. From 2002 to 2012, the ISAS13 reanalysis is used, while during 2013, only the Near Real Time (NRT) Coriolis analysis was available. The NRT Coriolis product is computed with the ISAS-V5.1 tool and the ISAS09

reference climatology; ISAS13 reanalysis uses ISAS-V6 tool and the ISAS11 reference climatology ([Gaillard, 2012, ISAS Technical Report]; see also http://wwz.ifremer.fr/lpo/La-recherche/Projets-en-cours/GLOSCAL/Global-T-S-analysis/Methodology). For each month over the period 2002-2013, data from various sources are interpolated onto 152 standard depth levels between 0-2000 m depth and then optimally interpolated into 0.5°x0.5° fields. In order to obtain interannual-to-decadal variability of spiciness the temperature and salinity monthly gridded fields are linearly interpolated onto isopycnal surfaces, then the monthly climatological temperature and salinity averages over the period 2004-2013 are removed from the monthly isopycnal temperature and salinity [*Kolodziejczyk and Gaillard*, 2012]. In this study, the σ_θ=26.3 isopycnal layer is retained because it connects the Agulhas current layer and the Sub-Tropical Front (STF, *Belkin and Gordon*, 1996), thus included in the Southern Hemisphere 'Supergyre' ; and is located below the deepest mixed layer during the Argo period of observation. Also, this study focuses on the northward route of the pycnocline circulation in the context of the AMOC [*Gordon*, 1986], thus only the northern part of the SSA gyre feeding the South Atlantic western boundary current has been investigated. To better investigate the propagative signal of spiciness a positive trend of 0.005 pss/year has been removed from the isopycnal layer. This trend is observed over the whole width of the basin without east-west apparent geographical phase lag. The mean Montgomery potential and geostrophic velocities on isopycnal surfaces were computed following *McDougall and Klocker* [2010]. The reference level for mean geostrophic velocities between 2004 and 2013 is the surface dynamic topography MDT_CNES-CLS09 based on GRACE (Gravity Recovery and Climate Experiment), satellite altimetry and in situ measurements [*Rio et al.*, 2011] combined with AVISO Sea Level Anomalies (SLA) monthly averages [*Ducet et al.*, 2000] for the period 2004–2013.

Within the SSA pycnocline layer - here materialized by the isopycnal σ_θ=26.3 - the salinity interannual Standard Deviation (STD) exhibits the strongest variability along 12°S (Fig. 1b) at the location of the subsurface salinity maximum (Fig. 1a). It is probably due to the large variance associated with the tropical salinity front position. This region is not within the SSA gyre which is located south of roughly the 3 $m^{-2}.s^{-2}$ Montgomery function isopleth (thick black curve; Fig. 1). Indeed, the isopleths with values smaller than 3 $m^{-2}.s^{-2}$ are not connected with 'Supergyre' stream in the South Eastern Atlantic off the South African tip, and are therefore beyond the scope of this study. The mean circulation of the SSA gyre takes its source in the region of the Agulhas Retroflection (at about 50-100 m depth) near 39.5°S/18-20°E [*Dencausse et al.*, 2010ab], where salinities are relatively low both at surface and within the pycnocline. It then crosses the SSA below the Sea Surface Salinity (SSS) maximum (Fig. 1a) to the South American western boundary currents near 270-m depth (Fig. 1c). Along its stream lines the STD of salinity anomalies is observed to be close to 0.05 pss for the period 2002-2013 (Fig. 1b,c). In the SSA gyre between 3-5 $m^{-2}.s^{-2}$ stream functions, the averaged salinity STD is strongest just below the mixed layer near the western boundary (>0.12 pss). However, it also

shows a relatively homogeneous level around 0.02-0.06 pss within the layer σ_θ=26.0-26.5. In this layer, the STD decreases westward (Fig. 1bc) suggesting a westward attenuation of the spiciness signal similar to what is observed in the Pacific Ocean [*Kolodziejczyk and Gaillard*, 2012].

On the σ_θ=26.3 isopycnal within the 3-5 $m^{-2}.s^{-2}$ stream functions of the SSA gyre, a propagation of interannual-to-decadal spiciness anomalies is observed (Fig. 2). A negative anomaly starts off South Africa around 15°E in 2004-2005 (Fig. 2c) then propagates north-westward, and reaches the South American coast (~35°W) around 2009, nearly 5 years later (Fig. 2aef). At large scales its amplitude reaches about 0.06 to 0.08 pss. A lagged-correlation analysis reveals that it propagates at 0.04±0.02 $m.s^{-1}$ which is equal to the velocity of the mean gyre current computed from the present data set (that is 0.04±0.03 $m.s^{-1}$), consistently with previous model studies [*Lazar et al.*, 2001; *Weijer et al.*; 2002; *Haarsma et al.*, 2011]. This negative anomaly is preceded by shorter positive anomalies emanating off South Africa before 2004 and reaching 10°W in 2004. During 2008-2009 a second positive salinity anomaly appears off South Africa (Fig. 2a and e), which then propagates north-westward. It is followed by a smaller negative anomaly during 2010 (Fig. 2a). The propagation of the later can be tracked up to 0°E, where it gets lost. Finally, a third positive salinity anomaly is generated in 2011-2012, which propagates up to 20°W in late 2013. Since 2011 and up to late 2013, it is worth noticing that salinity anomalies can locally reach values up to 0.1 pss west of 15°W or around 5-10°W in 2013 (Fig. 2g), with no apparent connection with propagating patterns. This suggests an additional local generation of spiciness anomalies within the pycnocline from surface processes (Fig. 2a and g).

3 Spiciness variability modes

Within the SSA pycnocline, the observations of low-frequency spiciness signals between 2002-2013 suggest two modes of spiciness interannual-to-decadal variability. The first mode is a propagating mode associated with the density compensated thermohaline anomalies advected by the gyre circulation which emanates from the Agulhas Retroflection region. In Figure 3, the anomaly of averaged salinity in the upper ocean (between 0-200 m depth) within the 5-25°E/30-48°S box off South Africa reveals an increasing trend of salt content anomaly from 2002 to 2013 (about 0.003 pss/year, black curve, Fig. 3a and c). Note that the 5-25°E/30-48°S box is consistently sampled with Argo profiles during the period 2004-2013 (Fig. 3b). The detrended signal (Fig. 3a, bars) exhibits negative vertically averaged salinity anomalies mainly observed during the period 2004 to 2008 as seen previously, except during 2006. In contrast, positive anomalies are generally observed after 2008 until 2011, except shortly in early 2010 (Fig 3a), as seen in the previous section. During 2013, the isopycnal salinity anomaly is negative, while the vertical averaged salinity anomalies is negative during 2012-13. This suggests a small lag between isopycnal salinity and vertically averaged salinity (Fig. 2a

and Fig. 3a). This vertically averaged salinity interannual-to-decadal variability is generally consistent with the propagating salinity features observed on the σ_θ=26.3 isopycnal off South Africa (around 10-15°E in Fig. 2). The off-South African box is the region of the Agulhas Retroflection [*Dencausse et al.*, 2010ab] which brings warm and salty water from the Indian ocean shedding rings in the South Eastern Subtropical Atlantic [*Biastoch et al.*, 2008]. This suggests that warm and saline water leaking from the Agulhas current could follow the thermohaline low-frequency spiciness route in the SSA.

A second mode of spiciness variability in SSA probably results from direct spice injection in the interior pycnocline. The vertical thermohaline configuration of the South Atlantic SSS maximum is characterized by destabilizing vertical salinity gradient at the pycnocline depth, *i.e.* salinity increasing upward, which presents its maximum along the propagation path. Following *Yeager and Large* [2007], in the SSA, the penetrative convective mixing may be an efficient mixing process for spice injection during late winter. Under winter buoyancy loss, upright convection contributes to inject salt and heat below the deepest late winter mixed layer (during September in the SSA) in a Strongly Density Compensated (SDC) layer. This layer is characterized by high vertical Turner angle. The buoyancy flux is computed according to [*Foltz and McPhaden*, 2008]: $B_0=\alpha Q_0/(C_p) - \beta\rho SSS(E-P)$; B_0 is the surface buoyancy flux (in kg.m^{-2}.s^{-1}) ; $Q_0=\partial Q_{flux}/\partial z$ is the heat forcing, the divergence of the sum of penetrative solar radiation, longwave radiation and the latent and sensible heat flux; C_p is the heat capacity of the sea water; SSS the Sea Surface Salinity; *E-P* is the Evaporation minus Precipitation flux. Heat and freshwater fluxes are from monthly-averaged 0.75°x0.75° ERA-interim reanalysis gridded fields available between 2002-2013 (ERA-interim is provided by the European Center for Medium-Range Weather Forecasts (ECMWF)). At interannual scales, the late winter buoyancy loss anomalies are largely explained by the latent heat loss anomalies over the SSA (Fig. 4a), *i.e.* it is the anomalous seasonal cooling rather than freshwater loss that control the buoyancy loss. During the late winter, the mixed layer depth anomalies are consistent with buoyancy loss anomalies (Fig. 4ab; note that the abscissa axis is inverted in Fig. 4b), especially during late winter 2010 to 2013, where stronger buoyancy losses and deeper than usual mixed layers are observed to be correlated in space and time (Fig. 4c). This suggests larger mixing during these late winters, including convective mixing. On the σ_θ=26.3 isopycnal, from 2010, the Turner angle values exhibit values of more than 72° higher than usual over the whole width of the SSA, indicative of formation of SDC layer that last over several years (Fig. 4d). On the other hand, the SSS anomalies increase up to 0.2 pss after 2009. However, the SSS anomalies do not necessarily reflect salinity anomalies injection on the σ_θ=26.3 isopycnal (see Fig. 2), since the buoyancy loss may be primary controlled by the heat loss, thus destabilizing the ocean upper layer. The spice injection mechanism is thus likely to contribute to local generation of spiciness during the late Argo period. The local spiciness patches associated

with SDC layer may then combine with the propagating pattern and also propagate with the mean currents in the interior pycnocline. It is worth noticing that this high Turner angle value (>71.6°) also favors double diffusive convection, thus enhancing the downward diffusion of salt and destroying SDC layer during spring re-stratification [*Johnson*, 2006].

4 Discussion

Low frequency spiciness signals are observed to propagate in the SSA with the velocity of the mean gyre circulation on the σ_θ=26.3 isopycnal. Part of this signal is probably generated off South Africa in the Agulhas Retroflection region [*Lutjeharms and van Ballegooyen*, 1988; *Dencausse et al.*, 2010ab]. Qualitative consistency between the upper layer salinity in the Agulhas Retroflection region and propagation of more or less warm and salty water masses suggests that the spiciness signal could be a part of the Agulhas leakage in the SSA. However, over the whole SSA width, the spiciness interannual-to-decadal variability could be also affected by late winter spice injection at the base of the mixed layer and originated from the SSS maximum in the surface layer . The late winter spice injection manifests itself by the highest Turner angle values observed below the mixed layer in the interior pycnocline deeper than the σ_θ=26.3 isopycnal during September, and is driven by the atmospheric winter buoyancy loss interannual anomalies [*Yeager and Large*, 2007]. This process is able to explain the local increase of the positive spiciness anomaly in the interior pycnocline [*Kolodziejczyk and Gaillard*, 2012] especially during 2010-2013 over the SSA .

However, the permanent pycnocline signal could be affected by other processes that are not addressed in this study. The horizontal eddy mixing may contribute to diffuse the tracer properties between the gyre circulation and the low potential vorticity pool [*Rhines and Young*, 1982] located south of the 5.5 $m^{-2}.s^{-2}$ stream line. This could explain the intrusion of positive spiciness anomalies west of 0°E near the southern edge of the σ_θ=26.3 isopycnal. Moreover, in the Agulhas Retroflection region, atmospheric flux driven injection and adiabatic subduction process as described in *Laurian et al.* [2009] could also play a role in the generation of spiciness signals on the σ_θ=26.3. This is associated with surface SST anomalies and the meridional position of the outcropping isopycnal during the late winter. At the interannual time scale no evident correlation has been found between SST and pycnocline spiciness signals, but at longer time scales the position of the Sub-Tropical Front (STF) could influence the spiciness injection and subduction in the Agulhas Retroflection region [*Böning et al.*, 2008]. In the south-eastern SSA, the question of how the mesoscale Agulhas rings impact the larger spiciness anomalies is not addressed in this study. Therefore, more work is needed to better separate the larger scale atmospheric forcing to the mesoscale forcing of Agulhas Leakage in the south-eastern SSA.

The Agulhas leakage into the SSA pycnocline can also generate Rossby waves as suggested by *Biastoch et al*. [2008]. The long Rossby wave dynamics in the SSA pycnocline are not addressed in this study, since we only investigate the advective density-compensated component of the signal. However, in a model study *Weijer et al*. [*2002*] have shown a faster time of westward propagation for wave like signal in the SSA (about 2 years), that could not be misinterpreted with the spiciness signal. Further work is needed to study the different dynamical aspects of the low-frequency SSA pycnocline variability.

Eventually, some questions remain. In the south-eastern SSA, the potential link between the spiciness low-frequency variability and the intensity of the Agulhas leakage need to be further investigated. The later could be also influenced by the Southern Hemisphere westerlies [Biastoch et al., 2009]. The impact of the Agulhas leackage on the upper limb of the AMOC, in the upper ocean, also remains unclear [*Beal et al.*, 2011]. This study also demonstrates the necessity to further investigate the interaction that may take place between AMOC and the STC circulation [*Haseleger and Drijfhout*, 2006]. Indeed, this signal, reaching the western boundary currents, could circulate with the average flow, upwell in the eastern tropics [*Hazeleger et al.*, 2003], and affect tropical climate [*Haarsma et al.*, 2011]. However, the results of the present study also underline the probable important effect of air-sea interaction over the SSA (and over the Atlantic) which modulates the spiciness signal [*Weijer et al*., *2002*]. The large air-sea flux anomalies observed since late 2009 could result from the broader impact of 2009-2010 ENSO, through atmospheric teleconnection [*Colberg et al.*, 2004]. The precise air-sea interaction impact over the pycnocline thermohaline properties remains to be explored in the context of the interannual-to-decadal variability of South Atlantic STC and AMOC circulation.

Acknowledgment: Nicolas Kolodziejczyk is supported by a CNES grant (French Space Agency). The ISAS project was funded by Ifremer 'Ocean and climate project', the INSU-LEFE program and by CNES-TOSCA project 'SMOS'. For the period 2002-2012, the ISAS analysis data for this paper are available at the ISAS project page: http://wwz.ifremer.fr/lpo/La-recherche/Projets-en-cours/GLOSCAL/Global-T-S-analysis; data set: ISAS2013. Dataset name: D7CA2S0_*. For the year 2013, the ISAS analysis data are available at the Coriolis page: http://www.coriolis.eu.org/Data-Services-Products/View-Download/Browse-T-S-maps. Dataset: INSITU_GLO_TS_OA_OBSERVATIONS. Dataset name: OA_NRTOAGL01_*. The altimeter fields were produced by Ssalto/Duacs and distributed by Aviso with support from Cnes (http://www.aviso.altimetry.fr/duacs/). Dataset: monthly 1/3°x1/3° updated delayed time multi-mission map of sea level anomaly. Dataset name: dt_upd_gobal_merged_msla_h_* . MDT_CNES-CLS09 was produced by CLS Space Oceanography Division and distributed by Aviso with support from Cnes (http://www.aviso.altimetry.fr/). Dataset file:

MDT_CNES_CLS09_v1.1.nc. The ERA-interim reanalysis products are freely provided by European Centre for medium-range Weather Forecasts. ERA-interim dataset : http://www.ecmwf.int/research/era/do/get/era-interim. The authors wish to thanks Sabrina Speich and anonymous reviewers for their valuable comments that substantially improved this manuscript.

References:

Beal, L. M., W. P. M. De Ruijter, A. Biastoch, R. Zahn & SCOR/WGRP/IAPSO Working Group 136, (2011), On the role of the Agulhas system in the circulation and climate, *472*, 429-436.

Belkin, I. M., and A. L. Gordon, (1996), Southern Ocean fronts from the Greenwich merdian to Tasmania, *J. Geophs. Res.*, 101, C2, 3675-3696.

Biastoch, A., C. W. Böning, and J. R. E. Lutjeharms, (2009), Agulhas leakage dynamics affects decadal varaibility in the Atlantic overturning circulation, *Nature*, *456*, 489-492.

Böning, C. W., A. Dispert, M. Visbeck, S. R. Rintoul, and F. U. Schwarzkopf, (2008), The response of the Antarctic Circumpolar Current to recent climate change, 1, 864-869, doi: 10.1038/ngeo362.

Colberg, F., C. J. C. Reason, and K. Rodgers, (2004), South Atlantic response to El-Nino-Southern Oscillation induced climate variability in an ocean general circulation model, *J. Geophs. Res.*, 109, C12015, doi:10.1029/2004JC00230.

Dencausse, G., M. Ahran, and S. Speich, (2010a), Saptio-temporal characteristics of the Agulhas Retroflection, *Deep-Sea Res. I*, *57*, 1392–1405

Dencausse, G., M. Ahran, and S. Speich, (2010b), Routes of Agulhas rings in the southeastern Cape Basin, *Deep-Sea Res. I*, *57*, 1406–1421

De Ruijter, W. P. M., (1982), Asymptotic analysis of the Agulhas and Brazil current systems, *J. Phys. Oceanogr.*, 12, 361- 373.

Ducet, N., P.-Y. Le Traon, and G. Reverdin, (2000), Global high resolution mapping of ocean circulation from Topex/Poseidon and ERS-1 and -2, *J. Geophys. Res.*, 105 (C8), 19,477-19,498.

Foltz, G. R., and M. J. McPhaden, (2008), Seasonal mixed layer salinity balance of the tropical North Atlantic Ocean, *J. Geophys. Res.*, 113, C02013, doi:10.1029/2007JC004178.

Friocourt, Y., S. Drijhout, B. Blanke, and S. Speich, (2005), Water mass export from the Drake Passage to the Atlantic, Indian and Pacific oceans: a Lagrangian model analysis, *J. Phys. Oceanogr.*, *35*, 1206-1222.

Gaillard, F., E. Autret, V. Thierry, P. Galaup, C. Coatanoan, and T. Loubrieu, (2009), Quality Control of Large Argo Datasets, *J. Atmos. And Oceanic Tech.*, *26*, 337-351.

Gaillard, F., (2012), Isas-tool version 6 : Method and configuration. Tech. rep., IFREMER.

Gordon, A. L., (1986), Interocean exchange of thermocline water, *J. Geophys. Res.*, 91, 5037-5046

Gordon, A. L., (1996), *Communication between oceans*, *Nature*, 382, 399-400.

Haarsma, J. R., E. J. D. Campos, S. Drijhout, W. Hazeleger, and C. Severijns, (2011), Impacts of interruption of the Agulhas leakage on the tropical Atlantic in coupled ocean–atmosphere simulations, 36, 989-1003, doi:10.1007/s00382-009-0692-7.

Hazeleger, W., P. de Vries, and Y. Friocourt, (2003), Sources of the equatorial undercurrent in the Atlantic in a high-resolution ocean model, J. Phys. Oceanogr., 33, 677-693. doi:10.1175/1520-0485.

Hazeleger, W., S. Drijfhout, (2006), Subtropical cells and meridional overturning circulation pathways in the tropical Atlantic. *J. Geophys. Res.*, *111*, doi:10.1007/s00382-005-0047.

Johnson, G. C., (2006), Generation and Initial Evolution of a Mode Water θ-S Anomaly, *J. Phys. Oceanogr., 36*, 739-751.

Kolodziejczyk, N., and F. Gaillard, (2012), Interannual varaibility of spiciness in the Pacific pycnocline, *J. Geophys. Res., 117,* C12018*,* doi:10.1029/2012JC008365.

Kolodziejczyk, N., and F. Gaillard, (2013), Variability of the Heat and Salt Budget in the Subtropical South-Eastern Pacific Mixed Layer between 2004 and 2010: Spice Injection Mechanism, *J. Phys. Oceanogr., 43,* 1880-1898.

Lazar, A., R. Murtugudde, and A. J. Busalacchi, (2001), A model study of temperature anomaly propagation from subtropics to tropics within the South Atlantic thermocline, *Geophys. Res. Lett.*, *28*, 1,271-1,274.

Laurian, A., A. Lazar, and G. Reverdin, (2009), Generation mechanism of poleward propagating spiciness anomalies in the North Atlantic subtropical gyre, *J. Phys. Oceanogr.*, 39, 1003-1018.

Lutjeharms, J. R. E., (1987), Meridional heat transport across the Sub-Tropical Convergence by a warm eddy, *Nature*, 331, 251- 253.

Lutjeharms, J. R. E., and R. C. Van Ballegooyen, (1988), The Retroflection of the Agulhas Current. J. *Phys. Oceanogr.*, 18, 1570-1583. doi:10.1175/1520-0485(1988)018<1570:TROTAC>2.0.CO;2

McDougall, T. J., and A. Klocker, (2010), An approximate geostrophic streamfunction for use in density surface, *Ocean Modelling*, 32, 105-117.

Rio, M.-H., S. Guinehut, G. Larnicol, (2011), The New CNES-CLS09 global Mean Dynamic Topography computed from the combination of GRACE data, altimetry and in-situ measurement, *J. Geophys. Res.*, *116*, C017018, doi: 10.1029/2010JC006505.

Rhines, P. B., and W. R. Young, (1982),Homogenization of potential vorticity in planetary gyres, *J. Fluid Mech.*, *122*, 347-367.

Ruddick, B., (1983), A practical indicator of stability of the water column to double-diffusive activity, *Deep-Sea Res.*, *30A*, 1,105-1,107.

Rhines, P. B., and W. R. Young, (1982),Homogenization of potential vorticity in planetary gyres, *J. Fluid Mech.*, *122*, 347-367.

Rusciano, E., S. Speich and M. Ollitrault, (2012), Antarctic Intermediate Water dynamics, budget and fluxes. Interocean exchanges South of Africa. *J. Geophys. Res.* 117, C10010, doi:10.1029/2012JC008266.

St. Laurent, L., and R. W. Schmitt, (1999), The contribution of salt fingers to vertical mixing in the North Atlantic tracer release experiment, *J. Phys. Oceanogr.*, *29*, 1404-1424.

Sasaki, Y. N., N. Schneider, N. Maximenko, and K. Lebedev, (2010), Observational evidence for propagation of decadal spiciness anomalies in the North Pacific, *Geophys. Res. Lett.*, *37*, doi: 10.029/2010GL04716.

Speich, S., B. Blanke, et G. Madec, (2001), Warm and cold water paths of a GCM thermohaline conveyor belt. *Geophys. Res. Lett.*, 28, 311-314.

Speich, S., B. Blanke, and W. Cai, (2007), Atlantic Meridional Overturning and the Southern Hemisphere Supergyre. *Geophys. Res. Lett.*, 34, L23614, doi:10.1029/2007GL031583.

Veronis, G., (1972), On properties of seawater defined by temperature, salinity and pressure, *J. Mar. Res.*, *30* (2), 227-255.

Weijer, W., W. P. M. De Ruijter, A. Sterl, S. S. Drijfhout,(2002), Response of the Atlantic overturning circulation to South Atlantic sources of buoyancy, *Global and Planetary Change*, *34*, 293-311

Yeager, G. S., and W. G. Large, (2007), Observational Evidence of Winter Spice Injection, *J. Phys. Oceanogr.*, *37*, 2895-2019.

Zhang, Dongxiao, Michael J. McPhaden, William E. Johns, (2003), Observational Evidence for Flow between the Subtropical and Tropical Atlantic: The Atlantic Subtropical Cells. *J. Phys. Oceanogr.*, *33*, 1783–1797

Figures:

Figure 1: (a) Mean salinity and (b) STD of interannual salinity anomalies over the period 2002-2013 on the σ_θ=26.3 isopycnal (in pss; color). For both (a) and (b) mean Sea Surface Salinity (in pss; thin black contours); mean Montgomery function isopleths (in $m^2.s^{-2}$, in gray contours) whereas the 3 and 5 $m^2.s^{-2}$ Montgomery function isopleths are in thick black contours. (c) STD of interannual isopycnal salinity anomalies (in pss) over the period 2002-2013 as a function of longitude (in °) and potential density anomalies (in $kg.m^{-3}$). Mean isopycnal depths are in thin black contours (in m depth), and the maximum late winter mixed layer depth position is in thick dashed dotted black contour. The thick red line materialized the σ_θ=26.3 isopycnal.

Figure 2: (a) Distance-time diagram of detrended salinity anomaly (in pss) on σ_0 = 26.3 surface averaged between the 3-5 $m^2.s^{-2}$ mean Montgomery function isopleth (see Fig. 2b-g). The distance is reported from the most equatorward outcrop position of the σ_0= 26.3 off South Africa towards the western boundary. Dashed black curves are the characteristics of the mean velocity along the given isopleth. The dots correspond to the available profile positions. The horizontal thin dashed lines materialize the September month of each year. The region with no data is hatched. (b-g) 2-years average of σ_0= 26.3 isopycnal interannual detrended salinity anomalies (in pss) over the period 2002-2013. The mean Montgomery function isopleths (in $m^2.s^{-2}$) are in thin black contours, but the 3 and 5 $m^2.s^{-2}$ Montgomery function isopleths are highlighted in thick black contours. The inset panels correspond to sections of the isopycnal 2-year average of interannual salinity anomalies (in pss) taken between the 3 and 5 $m^2.s^{-2}$ Montgomery function isopleths. The thick red line materializes the σ_θ=26.3 isopycnal. Mean isopycnal depths are in thin black contours (in m depth). The deepest late winter mixed layer is indicated in thick dashed dotted black contour.

Figure 3: (a) Mean Monthly anomalies of salinity averaged in the upper 200 meters (in pss) within the Agulhas box 5-25°E/30-48°S between 2002 and 2013 (see Fig. 3c). (b) Number of profiles available in the Agulhas box. (c) 10-year trends (2009-2013 minus 2008-2004) of salinity averaged in the upper 200 m depth over the Tropical-Subtropical South Atlantic.

Figure 4: (a) Atmospheric buoyancy flux anomalies (in $kg\ m^{-2}\ s^{-1}$, solid thick curve, anomalous losses are filled in

364 blue) and latent buoyancy flux (in $kg\ m^{-2}\ s^{-1}$, blue thin line); (b) mixed layer depth anomalies (in m
365 depth; note that the abcissa depth axis is inverted to make easier the comparison between Fig. 4a and b,
366 anomalously deep ML is filled in blue) averaged between 1000 and 4500 km and between the 3 and 5 $m^{-2}.s^{-2}$
367 Montgomery function isopleths between 2002 and 2013. (c) Distance-time diagram of atmospheric
368 Buoyancy flux anomalies (in $kg\ m^{-2}\ s^{-1}$; color shading) and mixed layer depth anomalies (contours in m
369 depth; black contours: positive anomalies; white contours: negative (shallow) anomaly; C.I.: 5 m). (d)
370 Distance-time diagram of SSS anomalies (in pss; color shading) and Turner Angle values greater than 72°
371 (hatched area). The dashed horizontal lines materialize the September month of each year (late winter).

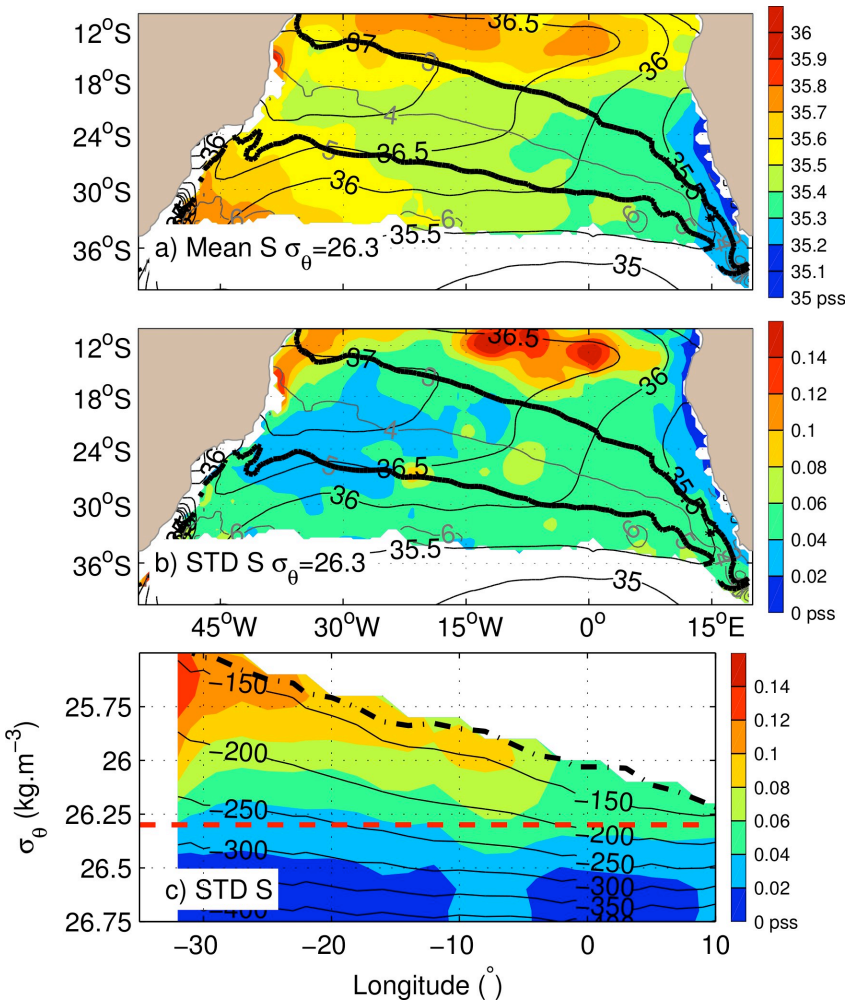

372

373 Figure 1: (a) Mean salinity and (b) STD of interannual salinity anomalies over the period 2002-2013 on the σ_θ=26.3
374 isopycnal (in pss; color). For both (a) and (b) mean Sea Surface Salinity (in pss; thin black contours); mean
375 Montgomery function isopleths (in $m^2.s^{-2}$, in gray contours) whereas the 3 and 5 $m^2.s^{-2}$ Montgomery function isopleths
376 are in thick black contours. (c) STD of interannual isopycnal salinity anomalies (in pss) over the period 2002-2013 as a
377 function of longitude (in °) and potential density anomalies (in $kg.m^{-3}$). Mean isopycnal depths are in thin black
378 contours (in m depth), and the maximum late winter mixed layer depth position is in thick dashed dotted black contour.
379 The thick red line materialized the σ_θ=26.3 isopycnal.

380

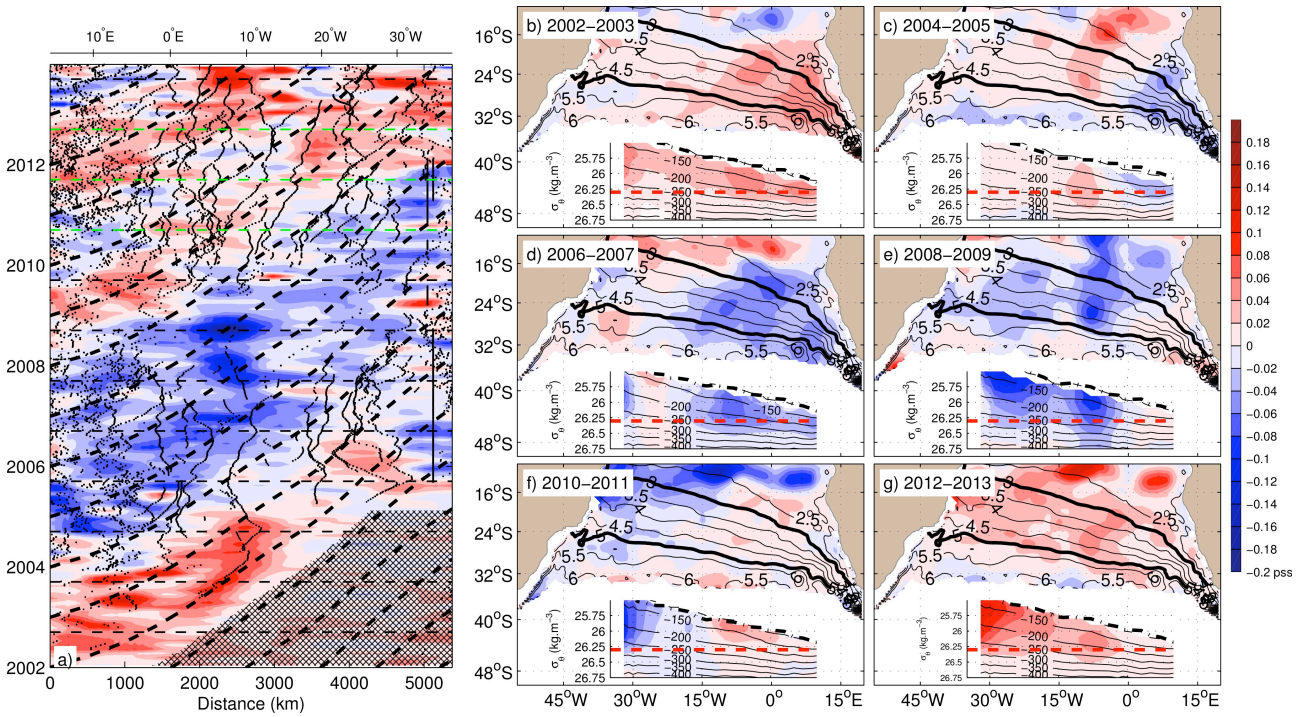

Figure 2: (a) Distance-time diagram of detrended salinity anomaly (in pss) on $\sigma_\theta = 26.3$ surface averaged between the 3-5 $m^2.s^{-2}$ mean Montgomery function isopleth (see Fig. 2b-g). The distance is reported from the most equatorward outcrop position of the $\sigma_\theta = 26.3$ off South Africa towards the western boundary. Dashed black curves are the characteristics of the mean velocity along the given isopleth. The dots correspond to the available profile positions. The horizontal thin dashed lines materialize the September month of each year. The region with no data is hatched. (b-g) 2-years average of $\sigma_\theta = 26.3$ isopycnal interannual detrended salinity anomalies (in pss) over the period 2002-2013. The mean Montgomery function isopleths (in $m^2.s^{-2}$) are in thin black contours, but the 3 and 5 $m^2.s^{-2}$ Montgomery function isopleths are highlighted in thick black contours. The inset panels correspond to sections of the isopycnal 2-year average of interannual salinity anomalies (in pss) taken between the 3 and 5 $m^2.s^{-2}$ Montgomery function isopleths. The thick red line materializes the σ_θ=26.3 isopycnal. Mean isopycnal depths are in thin black contours (in m depth). The deepest late winter mixed layer is indicated in thick dashed dotted black contour.

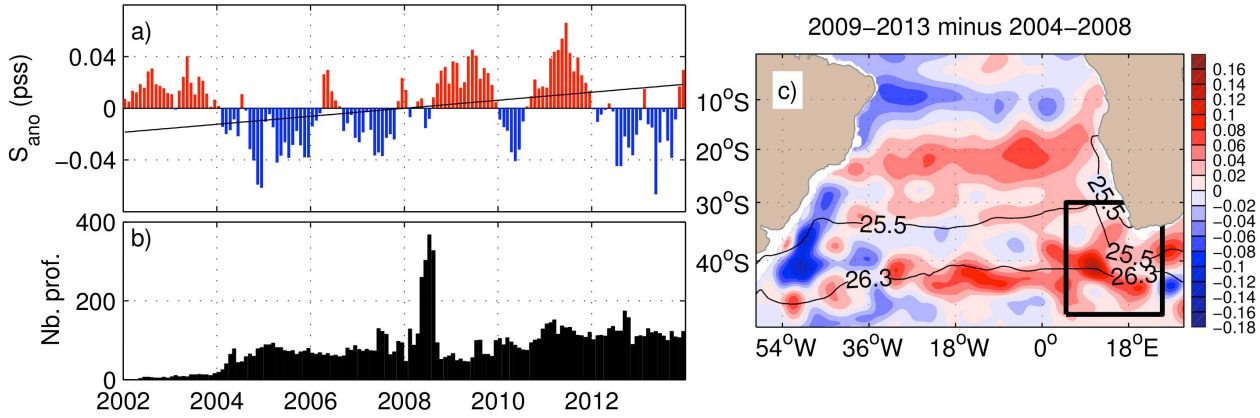

395

396 Figure 3: (a) Mean Monthly anomalies of salinity averaged in the upper 200 m depth (in pss) within the Agulhas box 5-
397 25°E/30-48°S between 2002 and 2013 (see Fig. 3c). (b) Number of profiles available in the Agulhas box.
398 (c) 10-year trends (2009-2013 minus 2008-2004) of salinity averaged in the upper 200 m depth over the
399 Tropical-Subtropical South Atlantic.

400

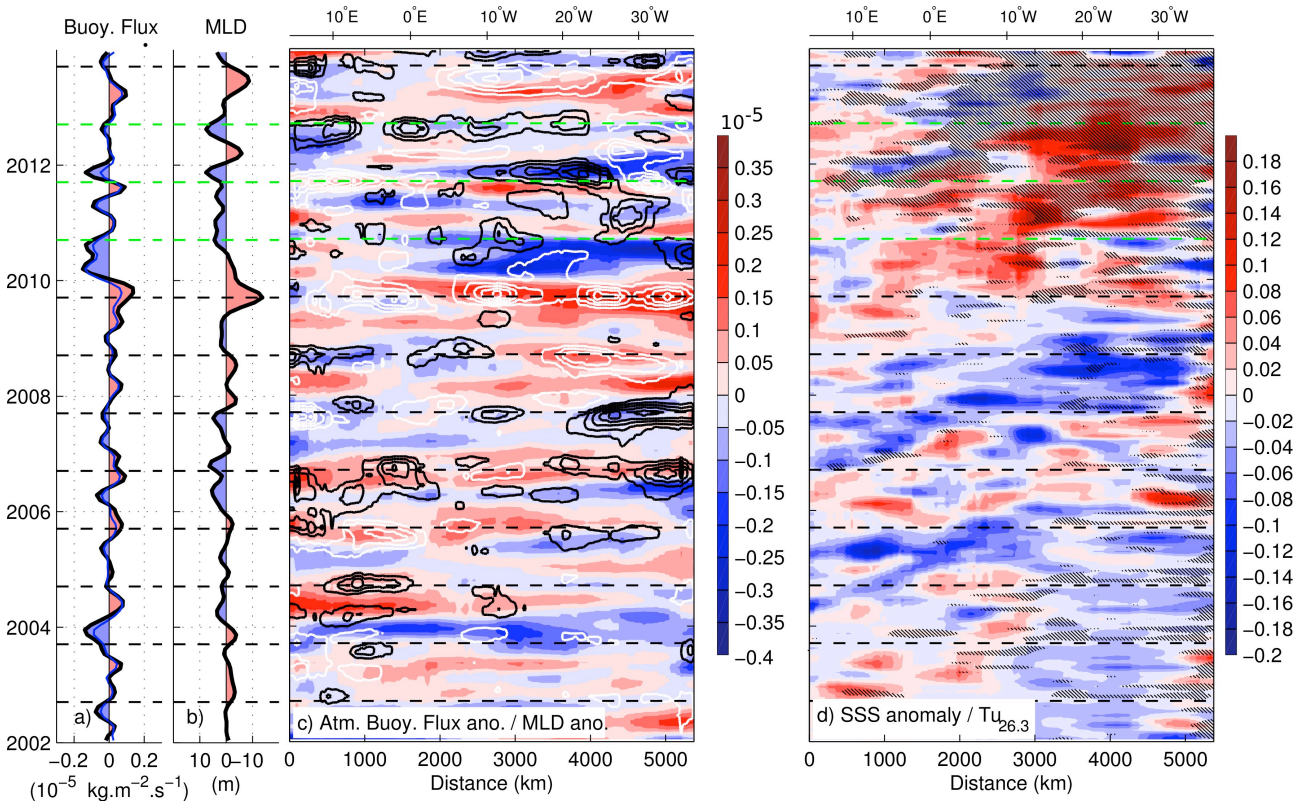

Figure 4: (a) Atmospheric buoyancy flux anomalies (in $kg\ m^{-2}s^{-1}$, solid thick curve, anomalous losses are filled in blue) and latent buoyancy flux (in $kg\ m^{-2}s^{-1}$, blue thin line); (b) mixed layer depth anomalies (in m depth; note that the abcissa depth axis is inverted to make easier the comparison between Fig. 4a and b, anomalously deep ML is filled in blue) averaged between 1000 and 4500 km and between the 3 and 5 $m^{-2}.s^{-2}$ Montgomery function isopleths between 2002 and 2013. (c) Distance-time diagram of atmospheric Buoyancy flux anomalies (in $kg\ m^{-2}s^{-1}$; color shading) and mixed layer depth anomalies (contours in m depth; black contours: positive anomalies; white contours: negative (shallow) anomaly; C.I.: 5 m). (d) Distance-time diagram of SSS anomalies (in pss; color shading) and Turner Angle values greater than 72° (hatched area). The dashed horizontal lines materialize the September month of each year (late winter).